IEEE Photonics Journal
An IEEE Photonics Society Publication

Fast Photon-Counting Imaging With Low Acquisition Time Method

Volume 13, Number 3, June 2021

Kangjian Hua
Bo Liu
Zhen Chen
Huachuang Wang
Liang Fang
Yun Jiang

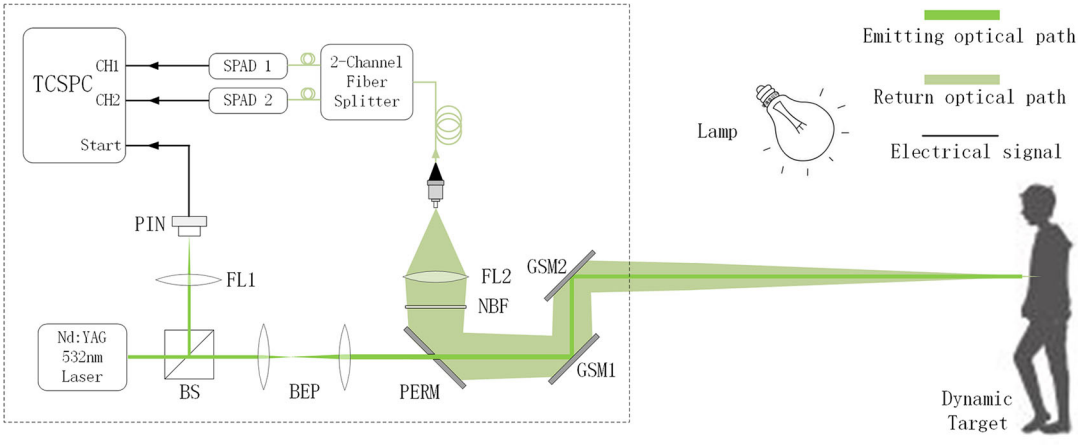

DOI: 10.1109/JPHOT.2021.3084171

Fast Photon-Counting Imaging With Low Acquisition Time Method

Kangjian Hua,[1,2,3] **Bo Liu**,[1,2,3] **Zhen Chen**,[1,2]
Huachuang Wang,[1,2] **Liang Fang**,[1,2] **and Yun Jiang**[1,2,3]

[1]Key Laboratory of Science and Technology on Space Optoelectronic Precision Measurement, Chinese Academy of Sciences, Chengdu 610209, China
[2]Institute of Optics and Electronics,Chinese Academy of Sciences, Chengdu 610209, China
[3]University of Chinese Academy of Sciences, Beijing 100049, China

DOI:10.1109/JPHOT.2021.3084171

Manuscript received March 11, 2021; revised May 17, 2021; accepted May 24, 2021. Date of publication May 26, 2021; date of current version July 2, 2021. This work was supported in part by the National Natural Science Foundation of China under Grant 61805249, and in part by the Youth Innovation Promotion Association of the Chinese Academy of Sciences under Grant 2019369. Corresponding author: Bo Liu (e-mail: boliu@ioe.ac.cn).
This article has supplementary downloadable material available at https://doi.org/10.1109/JPHOT.2021.3084171, provided by the authors.

Abstract: Photon-counting LIDAR has effective ability to detect significantly weak echo. However, for imaging application, it typically needs a long acquisition time to obtain sufficient counts to reconstruct clear depth image, which obviously limits imaging efficiency and prevents its wide deployment. In this paper, we proposed a low acquisition time photon-counting imaging method based on two single element SPADs and pixel scanning structure. Compared to fast imaging with SPAD array, the method has low requirement on laser energy and can obtain depth image with arbitrary pixel resolution. Experiment result demonstrates its feasibility and a dynamic target can be clearly captured by the system with our specifically designed reconstruction algorithm. We also detailly investigated the working conditions for the method. It reveals more than 2 echo photons per pulse would be enough to reconstruct clear depth image even when noise is intensive. Restricted to our 10 KHz laser source, the result only exhibited 1 frame per second(fps) imaging with pixel resolution of 100∗100. If a common 10 MHz laser is adopted, 512∗512 pixels resolution images can be captured at the rate of nearly 40 fps.

Index Terms: Photon-counting, low acquisition time, imaging efficiency, two SPADs.

1. Introduction

Photon-Counting imaging with time-correlated single-photon counting (TCSPC) technique recently has obtained intensive research interests in many applications [1]–[5]. Such photon-counting imager or photon-counting imaging LIDAR with single photon avalanche diode (SPAD) has ability to detect the incident of a single photon, which makes it suitable for scenarios where echo photon level is restricted such as remote sensing [6] or biomedicine fluorescent imaging [7].

For photon-counting LIDAR, echo is extremely weak and arrivals of echo photons are discrete and sparse events. Consequently, the flux of photons is generally modeled as Poisson point stochastic process [8], [9] and accordingly, for each laser pulse, signal count might not always appear. Instead, there are chances that noise counts generated from background light or detector dark current would show up. To suppress false alarm, it is typical for photon-counting LIDAR to

detect one pixel with hundreds to thousands of laser pulses to acquire adequate data to form counts histogram. Traditional linear LIDAR is not able to operate in such low echo level and its detector is linear photoelectric detector whose output voltage is linearly proportional to input echo intensity. In contrast, for linear LIDAR, transmitting one pulse would be enough to retrieve depth of one pixel.

Due to the unique operating manner, photon-counting LIDAR generally needs long acquisition (integration or dwell) time to complete imaging task, which obviously limits its imaging efficiency, e.g., as long as several seconds or even several minutes are required to generate a single frame of depth image. Many researches have been conducted to improve photon-counting imaging efficiency [10]–[17]. For example, A. Kirmani proposed first photon imaging (FPI) which only utilized the first photon count to reconstruct depth and intensity images [10], [11] and therefore the method could largely reduce imaging time. J. Rapp developed an unmixing method which exploits different statistics properties of signal and noise to design a special window censor approach to recover images with sparse photon-counting data [12]. Y. Altmann explored the correlations of adjacent pixels by introducing Markov random field and with these correlations, the method could restore images with fewer counts [13]. Although these methods could reconstruct images with much less data, their acquisition times are still fairly too long for some applications and imaging efficiency could be further improved. A. Maccarone exhibited the experiment to image rotating flange with SPAD array [18]. Parallel structure of SPAD array allows simultaneous acquisition for the whole of pixels and thusly total imaging time can be greatly decreased to capture moving target. However, illumination used for SPAD array should be flood illumination to cover the whole scene and therefore, compared with point scanning illumination which focuses its energy into a single point spot, such flood illumination would require much higher laser energy to achieve long range. Besides, large pixel scale SPAD array is not commercially available at present time.

Currently, the mainstreaming method to obtain large scale photon-counting images is to scan pixels consecutively. The aim of our work in this paper is to propose a low acquisition time photon-counting imaging method based on point scanning structure. The main difficulty of improving imaging efficiency for scanning structure is its serial detections of pixels, which results in large total acquisition time. However, if integration time for each pixel can be reduced, the total acquisition time thusly would be significantly decreased. The proposed method is to detect each pixel with as few as one pulse illumination, with the purpose of reducing total acquisition time as much as possible. To achieve it, a 2-channel 50:50 fiber splitter was used to separate echo into two portions to trigger two SPADs simultaneously. Two SPADs can provide double counts data compared with single SPAD.

However, with only one pulse illumination many pixels would have no counts at all, although counts data has been doubled. Besides, some counts of pixels would be noise counts which prevent us from reconstructing accurate depth images. To solve these two problems, a reconstruction algorithm that borrows counts from neighbor pixels and filters outlier counts has been developed. With two SPADs structure and specially designed reconstruction algorithm, our photon-counting LIDAR has ability to perform low acquisition time photon-counting imaging. The experiment demonstrated 1 frame per second (fps) imaging result on a moving man with resolution of $100*100$ pixels using 10 KHz repetition rate laser source. The movement of the target can be clearly identified in imaging result and it revealed that our method is able to effectively reduce acquisition time. Discussion has been conducted to investigate working conditions for our method and it indicates when echo reaches 2 photons per pulse, reconstructed image would be quite clear even when noise is intensive. The result also indicates if an MHz laser source which is largely available at present time was adopted, the frame rate and image size could be much larger, e.g., $512*512$ pixels size with 40 fps if a 10 MHz laser source is used.

2. System Description

The proposed low acquisition time photon-counting imaging system is demonstrated in Fig. 1.

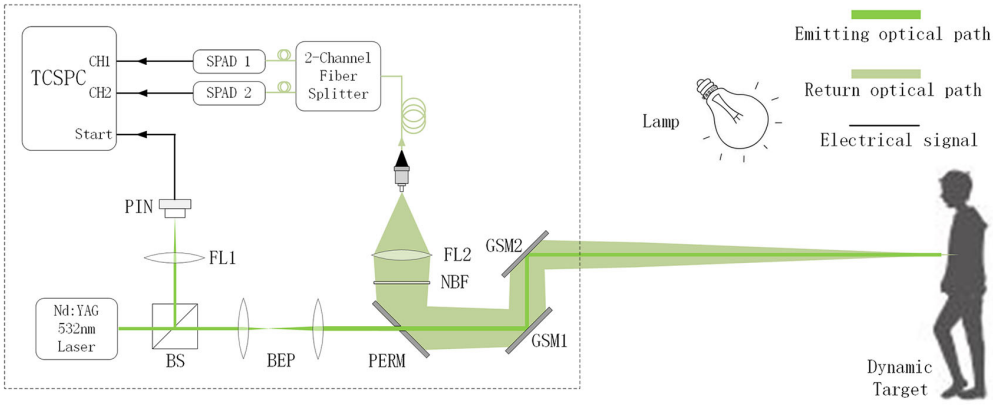

Fig. 1. Proposed low acquisition time photon-counting imaging system which comprises a Nd:YAG 532nm laser source, a PIN module, a 2-channel fiber splitter, two SPADs, a TCSPC module, a collimation lens(CL), a beam splitter (BS), two focus lenses(FL1 and FL2), a beam expander package(BEP), a perforated mirror (PERM), a narrow bandwidth filter(NBF) and two galvo scanning mirrors(GSM1 and GSM2).

Inside the dashed box is our imaging system. The system has been specially modified for low acquisition time photon-counting imaging application from our previously reported photon-counting devices [19], [20]. The laser (CryLaS FDSS532) emits periodical pulses at the repetition of 10 KHz with 1.3ns full width at half maximum (FWHM) pulse width. Beam splitter (BS) separates the energy of the laser beam into two portions. The 1% portion is to trigger PIN module as the start signal and the other 99% portion transmits through BS and then enters beam expander package (BEP) where laser pulse divergence is further lowered down. Afterwards, the beam would travel through the central hole of a perforated mirror (PERM) and then emit out with two galvo scanning mirrors (GSM1 and GSM2) (Thorlabs GVS012). On the contrary, the back reflected echo would largely be deflected into focus lens 2 (FL2) by PERM and eventually into 2-channel fiber splitter. The splitter would evenly divide the echo into two parts and each part is coupled with a SPAD detector. The two SPADs simultaneously detect echo photons and the generated counts would be registered by TCSPC (Siminics FT1020).

As can be noticed, co-axial configuration is adopted in our photon-counting LIDAR system. There are many reasons to use such configuration and the most advantage is that once we have completed the alignment of emitting and receiving optical path, it would require no alignment afterwards no matter how long the target is. Besides, compared with non-co-axial configuration, receiving field of view (FOV) for co-axial system can be as small as divergence of emitting beam to only cover laser spot, which can avoid additional background noise.

The target is a man who would walk around and wave hands during imaging process. The man serves as the dynamic target at a range of $\sim$10m. The purpose of experiment is to verify the feasibility of our low acquisition time photon-counting imaging method and to make experiment more impressive, the system is to capture depth image of dynamic scene. The whole of experiment was conducted in dark condition and a lamp was used as noisy background source.

The key modification of the system is the separation of echo into two channels. The underlying purpose is to expect more counts data. For each scanning pixel, we aim to obtain its depth information by only a single pulse illumination, namely, the accumulation number of each pixel for our fast photon-counting imaging LIDAR is 1.

3. Low Acquisition Time Photon-Counting Imaging Algorithm

The incidence of echo photons is generally modeled as a Poisson process. As has been mentioned in Section 2, echo photons would be separated evenly into two portions and such separation is

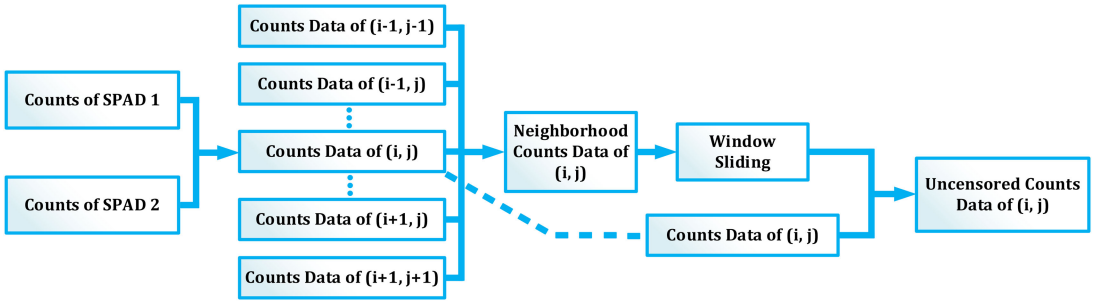

Fig. 2. Flowchart of proposed low acquisition time photon-counting imaging censor algorithm.

actually called Poisson thinning [21]. According to Poisson theory, Poisson thinning is to sort every count into different types with preset probabilities. Our separation is, in fact, a two-type Poisson thinning with equal probabilities for two types. The thinned processes are also Poisson processes with rate as $\lambda/2$ where λ is originally unseparated Poisson rate. More importantly, although these two thinned Poisson processes are from the same original Poisson process, they are actually independent with each other [21] and thusly we can treat the detection process of each SPAD independently.

For pixel (i, j), counts data of two channels are combined together as raw data $T^{i,j} = \{t_1^{i,j}, t_2^{i,j}, \ldots, t_k^{i,j}\}$ where superscript (i, j) denotes i-th row j-th column pixel, k is the combined number of counts and t represents time tag of count. For a single pulse illumination, there would be at most 2 signal counts. There are also chances that no signal photons would be detected or signal counts are submerged in noise counts. Generally, such little signal counts data is not adequate to recover clear depth image. To distinguish signal counts from noise counts, we proposed that each pixel should borrow counts from its adjacent pixels, which is an exploitation of pixel correlations in natural images. More specifically, for pixel (i, j), counts of its 3×3 neighbor pixels (including itself) are combined to form neighborhood counts data $T_{nei}^{i,j} = \{T^{m,n} | i-1 \leq m \leq i+1,\ j-1 \leq n \leq j+1\}$. Because signal counts would cluster within instrument response function (IRF) width while noise counts would distribute uniformly through the whole of time, we designed a censor algorithm to filter out noise counts. A window whose width is 4σ (σ is root mean square width of IRF) is utilized to slide from the first count of $T_{nei}^{i,j}$ to the last and at a certain position, this window would include the most counts and its corresponding position would be recorded. Then, for original $T^{i,j}$ pixel data, counts outside of window would be censored. The essence of the algorithm is the assumption that adjacent pixels have similar depth values. By borrowing counts data from adjacent pixels, a much larger neighborhood dataset is formed to indicate where counts cluster together and the position of window describes this cluster. Consequently, counts outside of cluster(window) is deemed as noise. Window width is set as 4σ for the reason that $\pm 2\sigma$ range would cover 95% signal counts for IRF Gaussian waveform. Such parameter can include the most of signal counts while avoid too many noise counts. The flowchart of the censor algorithm is demonstrated in Fig. 2.

To better demonstrate censor algorithm, a more detailed diagram is presented in Fig. 3. For pixel (i, j), counts of SPAD1 and SPAD2 are combined together as raw counts data which is highlighted in dashed green box. Counts of (i, j) and its 3×3 neighbor pixels are further combined to form neighborhood counts data. 4σ wide window slides through each count and record the position where the window includes the most counts. Finally, for raw counts of (i, j), counts out of the window are censored. In this way, each pixel would be checked to filter out potential noise.

After censoring, for pixel (i, j), mean value of its uncensored counts $T_u^{i,j} = \{t_1^{i,j}, \ldots, t_l^{i,j}\}$ is calculated as the initial estimated time of flight $\hat{T}^{i,j}$ where l is the number of uncensored counts.

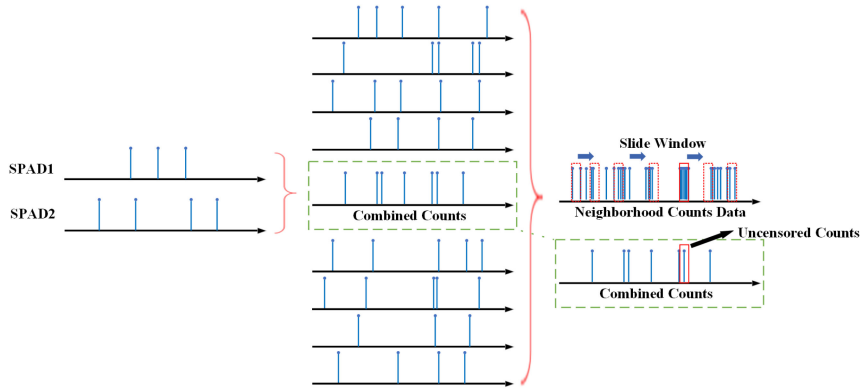

Fig. 3. Detailed diagram of proposed low acquisition time photon-counting imaging censor algorithm.

Estimated depth value $\hat{Z}^{i,j}$ is retrieved by multiplying $\hat{T}^{i,j}$ with $c/2$ where c is the speed of light.

$$\hat{Z}^{i,j} = \frac{c}{2}\hat{T}^{i,j} = \frac{c}{2l}\sum_{w=1}^{l} t_w^{i,j}, \tag{1}$$

However, it would be possible for a pixel to have no uncensored count (namely, $T_u^{i,j} = \emptyset$) and thusly the depth value would be empty. For this situation, empty depth value would be replaced with median value of its 3×3 neighborhood depths. If all of its surrounding 3×3 neighborhood pixels have empty values, neighborhood range would continue to expand until there is at least one non-empty value, e.g., neighborhood range would expand to 4×4 if all 3×3 pixels have empty depths and it would further expand to 5×5 if neither of 4×4 pixels have depths and so on.

After replacement, each pixel has a depth value and total variation (TV) constraint is applied to depth image to improve quality [22], [23]

$$Z = \arg\min_{Z} \left[\left(Z - \hat{Z} \right)^2 + \alpha TV\left(Z\right) \right], \; Z > 0, \tag{2}$$

where TV restrains depth image to be smooth and is defined as [22]

$$TV\left(Z\right) = \sum_{i=1}^{M-1}\sum_{j=1}^{N-1}\sqrt{\left(Z^{i,j} - Z^{i+1,j}\right)^2 + \left(Z^{i,j} - Z^{i,j+1}\right)^2} + \sum_{i=1}^{M-1}\left|Z^{i,N} - Z^{i+1,N}\right| + \sum_{j=1}^{N-1}\left|Z^{M,j} - Z^{M,j+1}\right|. \tag{3}$$

α is an empirical parameter to make a tradeoff between estimated depth and smoothness and (M, N) is the size of image. Experience indicates $\alpha = 2$ is suitable for a wide variety of scenarios with our system and its optimal value is the focus of our future work.

4. Experiment and Result

4.1 Calibration

There is no special requirement for two SPADs to be the same models from the same company. Two totally different SPADs can be applied in the system, e.g., PDM series \$PD-050-CTC-FC SPAD from Micro Photon Devices (MPD) corporation and SPCM series CD3565H SPAD from Excelitas corporation are applied as SPAD1 and SPAD2 respectively in our system. However, even when echo photons are from the same range, arrival times of them would not be same for two channels because the fiber lengths and electrical delays of SPADs may be different for manufacturing reasons. Besides, due to the internal optical path and TCSPC electrical delay, time of flight (TOF) would be overestimated with an offset. A calibration of TOF is needed to eliminate this offset and arrival time bias of two channels.

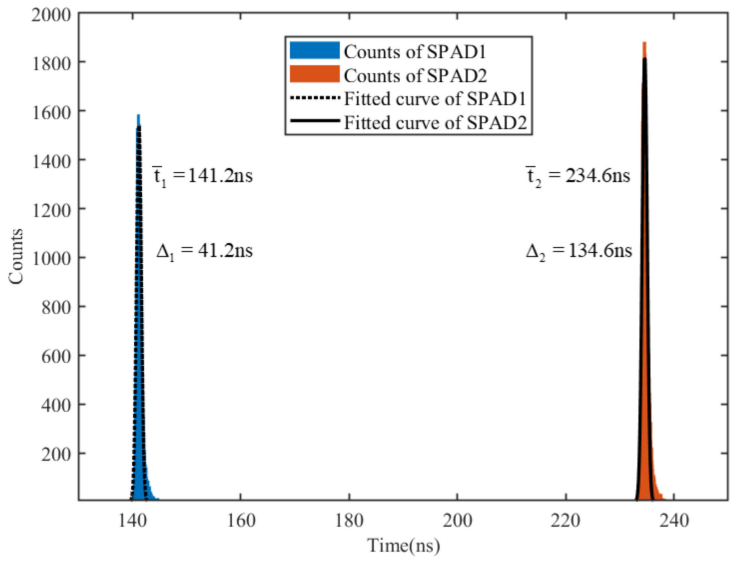

Fig. 4. Calibration of TOFs for two SPADs. Two histograms are generated from 1M pulses illuminations on a 15 meters away planar target.

A planar target with low reflectivity was placed accurately 1 5m away from front of the system and 1 M laser pulses were transmitted to illuminate the plane to generate two histograms as Fig. 4 indicates. Gaussian curves were utilized to fit counts histograms and the center values were 141.2 ns and 234.6 ns respectively. Since 15 m range corresponds to 100ns TOF, the calibration values for two channels are 41.2 ns and 134.6 ns respectively. Thereafter, times of recorded counts would subtract their corresponding calibration values.

4.2 Experiment Parameters

We set our image pixels size as 100∗100. Considering the repetition frequency of laser source used in system is 10 KHz, 1s acquisition would generate one frame of depth image, or the frame rate is 1 frame per second (FPS). The scanning angle is 53.756 mrad for X axis and 40.386 mrad for Y axis and thusly the scanning resolution is about 0.54 mrad for horizontal position and 0.40 mrad for vertical position. The time resolution of TCSPC was set to 64 ps. The target scene is a man walking before a background plate and the man is about 11m away from the system and the background plate is about 13 m. The experiment setup is displayed in Fig. 5. After the start of acquisition, the man would continuously change his body position and gesture.

4.3 Result

For more illustrative demonstration of experiment result on walking man, several short videos were uploaded to supplementary files. Nine frames of depth images from the first video are displayed in Fig. 6.

Fig. 6 or more straightforward supplementary videos clearly reveal the body movement and gesture action of the man. Through frames from Fig. 6, it indicated that the man slowly stretched his arms and raised his hands up above head and then put down his hands and rotated his body and eventually moved out of FOV with one hand waving around. For example, Frame1 exhibits the first frame of the video when the man put his hands close to body vertically and Frame37 demonstrates the man has fully raised his arms. With our low acquisition time photon-counting method, including two SPADs structure and reconstruction algorithm, the moving man can be clearly captured and

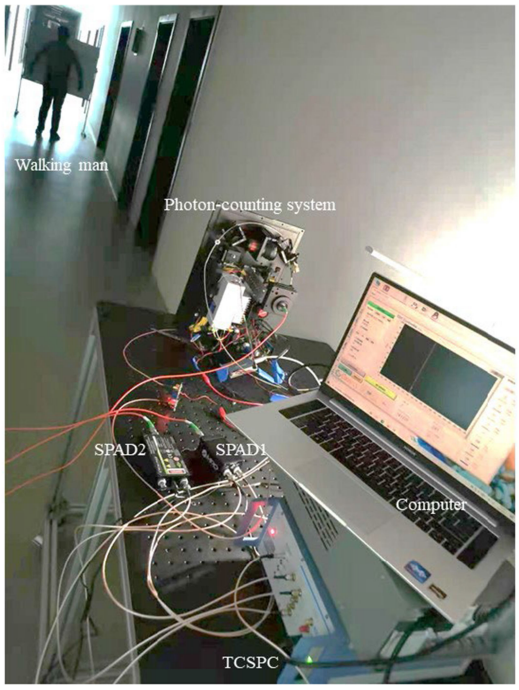

Fig. 5. Experiment setup which includes the photon-counting system, SPAD1, SPAD2, TCSPC, computer and a walking man.

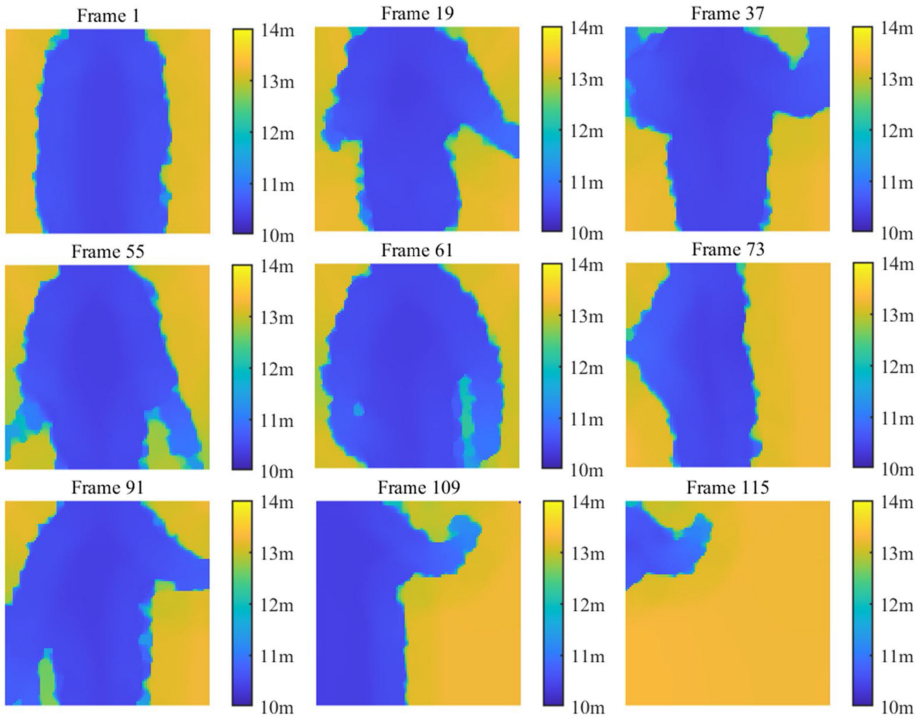

Fig. 6. Frames of depth images from the first supplementary video.

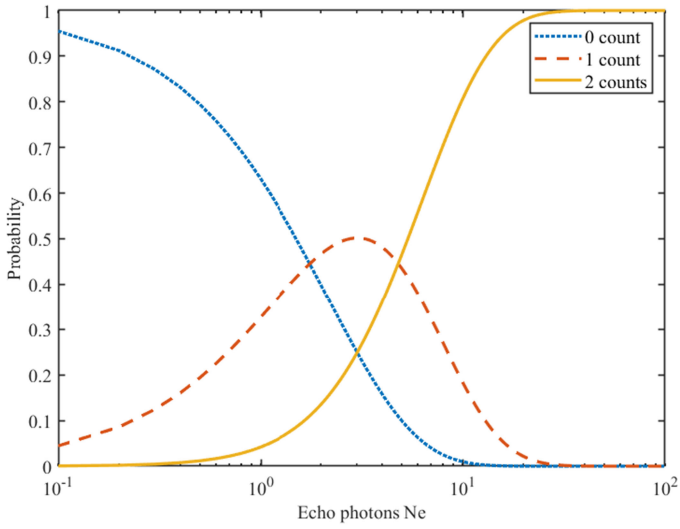

Fig. 7. Relationship between echo photons N_e and probabilities of 0 count, 1 count and 2 counts.

his body position can be easily identified which is exactly the favorable raw input for a variety of action recognition tasks.

5. Discussion

Although the system worked well enough to achieve our initial goal of capturing moving target, it is necessary to analyze the influence of echo and noise levels on image quality to provide information about working conditions for our method. Echo level primarily determines signal counts number for each pixel. We denote the number of echo photons per pulse as N_e and accordingly for each SPAD the number of echo photons per pulse is $N_e/2$. Here, the loss of fiber splitter is ignored for it is rather tiny. From Poisson process, the probability of detecting a signal count is

$$P_1 = 1 - \exp\left(-\frac{\eta_1 N_e}{2}\right), \tag{4}$$

$$P_2 = 1 - \exp\left(-\frac{\eta_2 N_e}{2}\right), \tag{5}$$

where η is photon detection efficiency (PDE) of the SPAD and P_1 and P_2 correspond to signal detection probabilities of SPAD1 and SPAD2 respectively. Using Eqs. (4)–(5) we can calculate the relationship between incident echo photons N_e and probabilities of combined signal counts numbers as Fig. 7. We set $\eta_1 = 0.42$ and $\eta_2 = 0.50$ in accordance with SPADs' parameter specifications.

From Fig. 7 two main conclusions can be drawn. The first is that with more echo photons, the probability of 2 counts increases. However, this trend would saturate after N_e reaches 20 which means too strong echo beam is not efficient and economical. The second is that fewer echo photons would make pixels tend to have no counts, which is significant to deteriorate image quality. Although our algorithm has designed the mechanism to borrow data from neighbor pixels to deal with empty problem, the image quality is expected to be greatly reduced if a large portion of pixels have no signal counts.

The key reason why two SPADs improve efficiency is that more signal counts could be expected during detection. For simplification, photon detection efficiencies of two SPADs are assumed to be the same and denoted as η. For a single SPAD, the detection probability of an echo count is $1 - \exp(-\eta N_e)$ and expectation of count number is

$$E_1(N_e) = 1 - \exp(-\eta N_e). \tag{6}$$

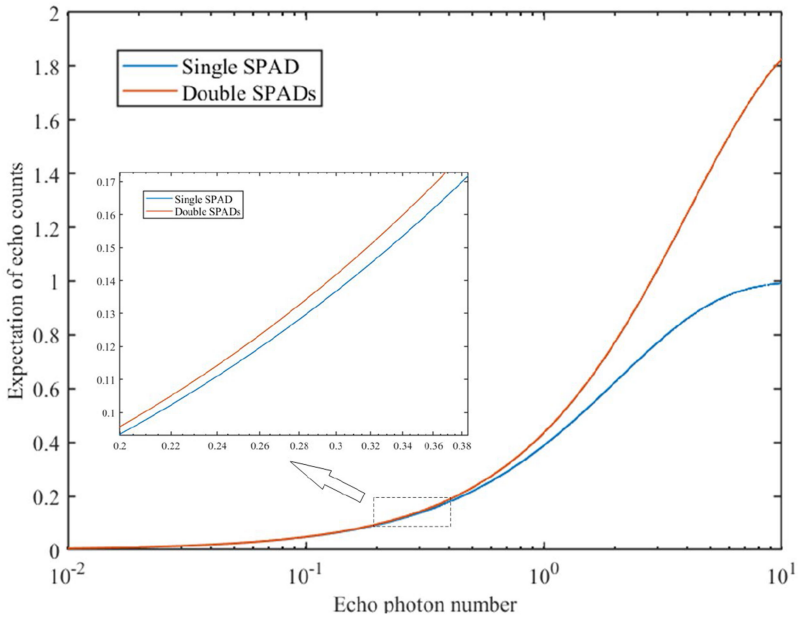

Fig. 8. Expectations of echo counts with variation of echo photon number N_e.

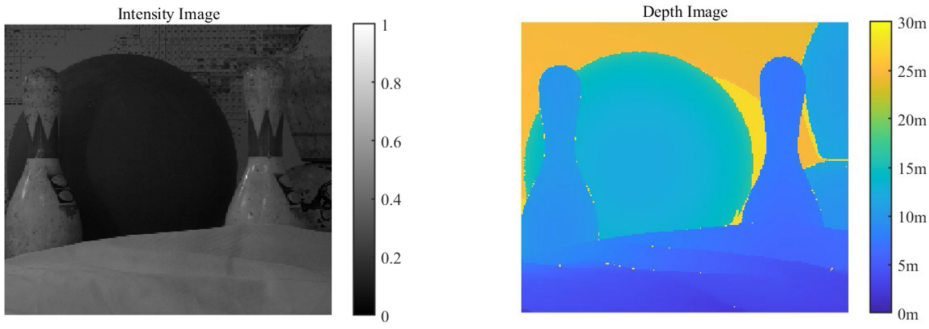

Fig. 9. Normalized intensity image and depth image for simulation. The truth depth and intensity of pixel (i, j) is denoted as $Z_{tru}^{i,j}$ and $I^{i,j}$ respectively.

For double SPADs, detection probabilities of an echo count and two echo counts are $2[1-\exp(-\frac{\eta N_e}{2})]\exp(-\frac{\eta N_e}{2})$ and $[1-\exp(-\frac{\eta N_e}{2})]^2$ respectively and therefore expectation of count number is

$$E_2 = 2\left[1-\exp\left(-\frac{\eta N_e}{2}\right)\right]\exp\left(-\frac{\eta N_e}{2}\right) + 2\times\left[1-\exp\left(-\frac{\eta N_e}{2}\right)\right]^2. \tag{7}$$

E_1 and E_2 are plotted in Fig. 8 with variation of echo photon number N_e where η is set as 0.50.

As Fig. 8 demonstrates, for one pulse illumination, expectation of double SPADs is larger than that of single SPAD, especially when echo photon N_e is large. When N_e is small, for example, N_e is fewer than 0.1, the advantage of double SPADs is negligible and if loss of fiber splitter is taken into account, double SPADs structure may cause negative effect.

To quantitatively explore how the echo and noise levels affect image quality, a simulation under different echo and noise conditions has been conducted. We use Bowling1 intensity and depth images from Middlebury dataset [24] for simulation. The normalized intensity image and its ground truth depth image are displayed in Fig. 9.

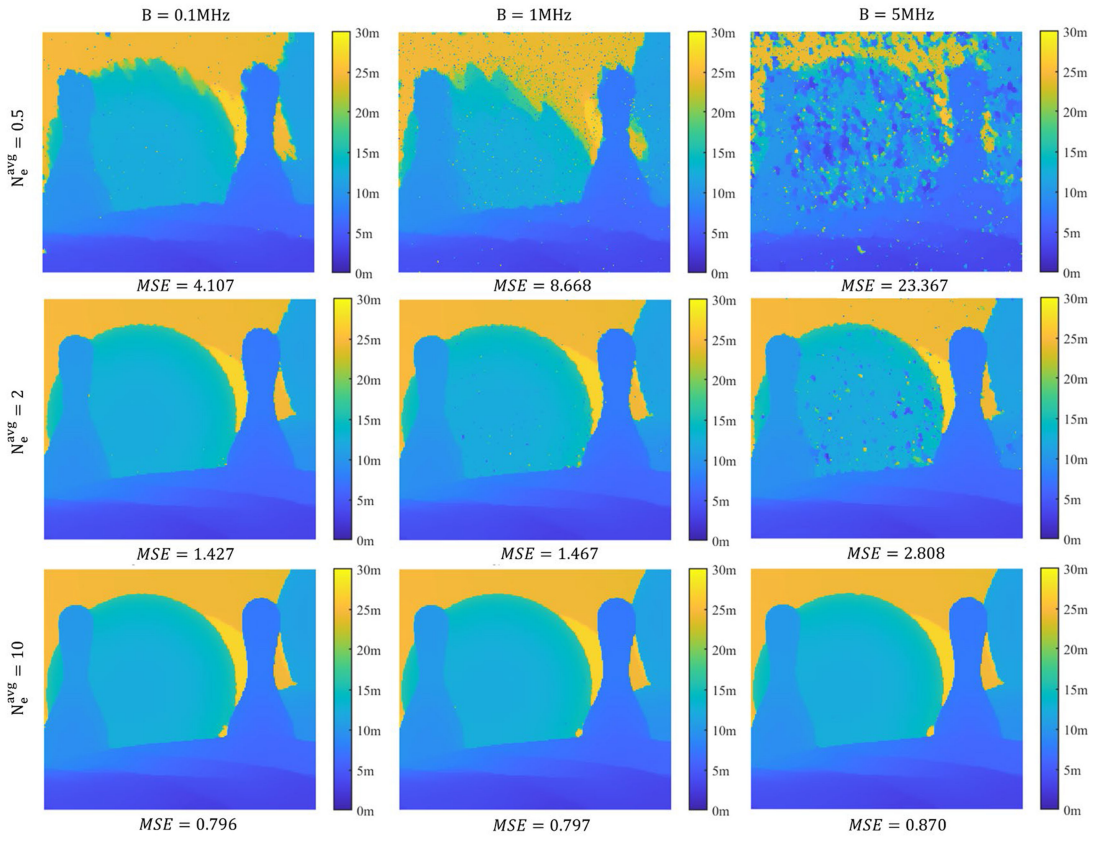

Fig. 10. Reconstruction result for a variety of signal and noise levels.

Echo photons for each pixel are linearly scaled to its intensity and the averaged echo photons number of the whole image are set as 0.5, 2 and 10 respectively. The background noise levels are set as 0.1 MHz, 1 MHz and 5 MHz. For pixel (i, j), two Poisson processes with rates as $\frac{\eta_1 I^{i,j} N_e^{avg}}{\sqrt{2\pi}\sigma I^{avg}} \exp(-\frac{(t-Z_{tru}^{i,j})^2}{2\sigma^2}) + \eta_1 B$ and $\frac{\eta_2 I^{i,j} N_e^{avg}}{\sqrt{2\pi}\sigma I^{avg}} \exp(-\frac{(t-Z_{tru}^{i,j})^2}{2\sigma^2}) + \eta_2 B$ are formed to generate photon counts for two SPADs where N_e^{avg} is aforementioned averaged echo photons number, I^{avg} is averaged image intensity, B. is background noise level and σ is RMS width of IRF which is set as 0.6ns to keep consistency with our system. Dark noise from SPAD is ignored for it is relatively small and gate time is 200ns for each pixel. The dead times of SPAD1 and SPAD2 are 77ns and 22ns respectively and therefore we would ignore the latter one if there are two counts generated within dead time. Reconstruction results are demonstrated in Fig. 10 with our algorithm. Mean square error (MES) is adopted to measure the image quality which is defined as

$$MSE = \frac{1}{MN}\left(Z^{i,j} - Z_{tru}^{i,j}\right)^2, \tag{8}$$

where (M, N) is aforementioned image size.

Fig. 10 reveals that our method has an outstanding tolerance to noise. Even noise level is as high as 5 MHz, a clear depth image with small MSE can be obtained on condition that echo photons are sufficient. However, when the echo photons number is small, the quality of image would rapidly become worse with the increasement of noise. To detailly investigate the trend of MSE on echo and noise levels, more sets of values are utilized in simulation and the result is plotted in Fig. 11.

From Fig. 11, it can be noticed that when echo photons are adequate, e.g., more than 2 photons per pulse, MSEs of reconstructed images would stay rather small even when noise level reaches

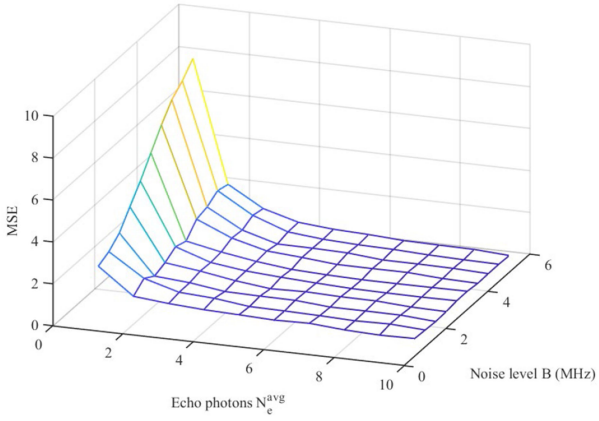

Fig. 11. Influence of echo photons number and noise levels on MSE.

higher and higher. However, if echo photons are insufficient, the image quality would become poor dramatically. The trend reveals that the method has a requirement for echo photons level and extremely low echo level such as excessively less than 1 photon per pulse is not suited for our fast imaging method, which has also been indicated in Fig. 8. Moreover, our method has an excellent robustness to noise once echo photons are enough and results demonstrate when echo photon number reaches 2 even intensive noise could hardly deteriorate image quality.

6. Conclusion

In this paper, we proposed a low acquisition time photon-counting imaging method which has ability to capture moving target. The method is based on two SPADs pixel scanning structure and a specifically designed algorithm, including borrow adjacent counts and TV denoising, is used to reconstruct depth frames. The experiment result of a moving man verified the feasibility of the method. Restricted to our 10 KHz laser source, the experiment only demonstrated 1 fps fast imaging with 100∗100 pixels resolution. However, if equipped with a 10 MHz pulsed laser which is largely available at present, 512∗512 pixels image can be obtained at nearly 40 fps. At last, we detailly discussed working conditions for our method and it indicates that when echo reaches 2 photons per pulse, the reconstructed image quality would remain fairly good even through the noise is intensive. The underlying reason to explain the feasibility of the method is that counts expectation of double SPADs is larger than that of single SPAD. Compared to fast imaging with SPAD array, our method has low requirement on laser energy and can achieve the goal of fast imaging with any preset pixel resolutions.

Acknowledgment

The authors wish to thank the anonymous reviewers for their valuable suggestions.

References

[1] Z. Li, *et al.*, "Photon-counting chirped amplitude modulation lidar with 1.5-GHz gated InGaAs/InP APD," *IEEE Photon. Technol. Lett.*, vol. 27, no. 6, pp. 616–619, Jan. 2015.
[2] A. M. Pawlikowska, A. Halimi, R. A. Lamb, and G. S. Buller, "Single-photon three-dimensional imaging at up to 10 kilometers range," *Opt. Exp.*, vol. 25, no. 10, pp. 11919–11931, May 2017.
[3] Z. Li, *et al.*, "Super-resolution single-photon imaging at 8.2 kilometers," *Opt. Exp.*, vol. 28, no. 3, pp. 4076–4087, Feb. 2020.
[4] L. Dai, J. Liu, K. Liang, R. Yang, D. Han, and B. Lu, "Realization of a time-correlated photon counting technique for fluorescence analysis," *Biomed. Opt. Exp.*, vol. 11, no. 4, pp. 2205–2212, Mar. 2020.

[5] A. Ingle, A. Velten, and M. Gupta, "High flux passive imaging with single-photon sensors," in *Proc. IEEE/CVF Conf. Comput. Vis. Pattern Recognit.*, Long Beach, CA, USA, 2019, pp. 6753–6762.
[6] Z. Li, *et al.*, "Single-photon computational 3D imaging at 45 km," *Photon. Res.*, vol. 8, pp. 1532–1540, Sep. 2020.
[7] F. M. D. Rocca, *et al.*, "Real-time fluorescence lifetime actuation for cell sorting using a CMOS SPAD silicon photomultiplier," *Opt. Lett.*, vol. 41, no. 4, pp. 673–676, Feb. 2016.
[8] D. G. Fouche, "Detection and false-alarm probabilities for laser radars that use Geiger-mode detectors," *Appl. Opt.*, vol. 42, no. 27, pp. 5388–5398 Sep. 2003.
[9] P. Gatt, S. Johnson, and T. Nichols, "Geiger-mode avalanche photodiode ladar receiver performance characteristics and detection statistics," *Appl. Opt.*, vol. 48, no. 17, pp. 3261–3276, Jun. 2009.
[10] A. Kirmani, *et al.*, "First-photon imaging," *Science*, vol. 343, no. 6166, pp. 58–61, Jan. 2014.
[11] A. Kirmani, D. Shin, D. Venkatraman, F. N. C. Wong, and V. K. Goyal, "First-photon imaging: Scene depth and reflectance acquisition from one detected photon per pixel," in *Proc. IEEE Int. Conf. Comput. Vis.*, Sydney, Australia, 2013, pp. 449–456.
[12] J. Rapp, and V. K. Goyal, "A few photons among many: Unmixing signal and noise for photon-efficient active imaging," *IEEE Trans. Comput. Imag.*, vol. 3, no. 3, pp. 445–459, Sep. 2017.
[13] Y. Altmann, X. Ren, A. McCarthy, G. S. Buller, and S. McLaughlin, "Robust Bayesian target detection algorithm for depth imaging from sparse single-photon data," *IEEE Trans. Comput. Imag.*, vol. 2, no. 4, pp. 456–467, Dec. 2016.
[14] Y. Kang, L. Li, D. Liu, D. Li, T. Zhang, and W. Zhao, "Fast long-range photon counting depth imaging with sparse single-photon data," *IEEE Photon. J.*, vol. 10, no. 3, Jun. 2018, Art. no. 7500710.
[15] A. Halimi, *et al.*, "Restoration of intensity and depth images constructed using sparse single-photon data," in *Proc. 24th Eur. Signal Process. Conf.*, Budapest, Hungary, 2016, pp. 86–90.
[16] D. Shin, A. Kirmani, V. K. Goyal, and J. H. Shapiro, "Photon-efficient computational 3D and reflectivity imaging with single-photon detectors," *IEEE Trans. Comput. Imag.*, vol. 1, no. 2, pp. 112–125, Jun. 2015.
[17] A. Kirmani, A. Colaço, F. N. C. Wong, and V. K. Goyal, "Exploiting sparsity in time-of-flight range acquisition using a single time-resolved sensor," *Opt. Exp.*, vol. 19, no. 22, pp. 21485–21507, Oct. 2011.
[18] A. Maccarone, F. M. D. Rocca, A. McCarthy, R. Henderson, and G. S. Buller, "Three-dimensional imaging of stationary and moving targets in turbid underwater environments using a single-photon detector array," *Opt. Exp.*, vol. 27, no. 20, pp. 28437–28456, Sep. 2019.
[19] K. Hua, B. Liu, L. Fang, H. Wang, Z. Chen, and Y. Yu, "Detection efficiency for underwater coaxial photon-counting lidar," *Appl. Opt*, vol. 59, no. 6, pp. 2797–2809, Mar. 2020.
[20] K. Hua, B. Liu, L. Fang, H. Wang, Z. Chen, and J. Luo, "Correction of range walk error for underwater photon-counting imaging," *Opt. Exp.*, vol. 28, no. 24, pp. 36260–36273, Nov. 2020.
[21] G. Last, and M. Penrose, *Lectures On the Poisson Process*. Cambridge, U.K.: Cambridge Univ. Press, 2017.
[22] A. Beck, and M. Teboulle, "Fast gradient-based algorithms for constrained total variation image denoising and deblurring problems," *IEEE Trans. Image Process.*, vol. 11, no. 18, pp. 2419–2434, Nov. 2009.
[23] L. I. Rudin, S. J. Osher, and E. Fatemi, "Nonlinear total variation based noise removal algorithms," *Phys. D*, vol. 60, pp. 259–268, 1992.
[24] D. Scharstein, and C. Pal, "Learning conditional random fields for stereo," in *Proc. IEEE Conf. Comput. Vis. Pattern Recognit*. Melbourne, VIC, Australia, 2007, pp. 1–8.